Discovery of a Peptide Nucleic Acid (PNA) aptamer for cardiac troponin I: Substituting DNA with neutral PNA maintains picomolar affinity and improves performances for electronic sensing with graphene field-effect transistors (gFET)

Teresa Rodrigues, Federica Curti, Yann R. Leroux, Alexandre Barras, Quentin Pagneux, Henri Happy, Christoph Kleber, Rabah Boukherroub, Roger Hasler, Stefano Volpi, et al.

Discovery of a Peptide Nucleic Acid (PNA) aptamer for cardiac troponin I: substituting DNA with neutral PNA maintains picomolar affinity and improves performances for electronic sensing with graphene field-effect transistors (gFET)

Teresa Rodrigues,[1,2] Federica Curti,[2,3] Yann R. Leroux,[4] Alexandre Barras,[1] Quentin Pagneux,[1] Henri Happy,[1] Christoph Kleber,[5] Rabah Boukherroub,[1] Roger Hasler,[2,5] Stefano Volpi[3], Maria Careri,[3] Roberto Corradini,[3*]and Sabine Szunerits,[1,5*] Wolfgang Knoll,[2,3,5*]

[1] *Univ. Lille, CNRS, Centrale Lille, Univ. Polytechnique Hauts-de-France, UMR 8520 - IEMN, F-59000 Lille, France*

[2] *AIT Austrian Institute of Technology GmbH, Biosensor Technologies, 3430 Tulln, Austria*

[3] *University of Parma Department of Chemistry, life sciences and Environmental Sustainability, 43124 Parma, Italy*

[4] *Univ. Rennes, CNRS, ISCR – UMR 6226, F-35000 Rennes, France*

[5] *Laboratory for Life Sciences and Technology (LiST), Faculty of Medicine and Dentistry, Danube Private University, 3500 Krems, Austria*

Abstract

DNA-based aptamers are widely employed as bioreceptors, owing to their tuneable affinity and specificity towards their targets. The use of peptide nucleic acids (PNAs) has instead proven challenging for this purpose, due to the absence of selection methods for the independent discovery of suitable receptors and due to the difficult mimicry of established DNA-based ones. Despite that PNAs exceed homologous DNA or RNA in terms of complementary base pairing, they can fail to reproduce alternative modes of binding because of their different structural features. The remarkable stability and charge distribution of PNAs could be beneficial to produce sensing bioreceptors, especially in the development of electronic devices such as field-effect transistor-based (FET) biosensors. We hereby report for the first time a high-affinity PNA aptamer for cardiac Troponin I (cTnI), a biomarker of acute myocardial infarction able to interact with this specific protein in the picomolar range. The PNA aptamer was immobilized onto a graphene-based FET (gFET) transducer, and its ability in the direct detection of cTnI was compared with that of a DNA-based one of the same sequences. Similar dissociation constants were recorded for both receptors in 0.01× PBS, as well as comparable detection limits of 6.0 ± 1.0 pg mL^{-1} (PNA aptamer) and 3.3 ± 0.7 pg mL^{-1} (DNA aptamer). Apart from the non-trivial demonstration that a PNA can behave as an aptamer, the tested receptor proved to be more consistent upon working in more complex biological matrices.

Keywords: Graphene-based field effect transistor, peptide nucleic acid, aptamer, cardiac troponin I, biosensor.

1. Introduction

The flexibility that nucleic acid aptamers offer in terms of chemical modification, together with their high affinity and selectivity for target analytes, render them suitable for a large variety of analytical applications, serving either as alternatives to antibodies or as unique receptors with peculiar properties [1-3]. The secondary structures of aptamers can, in addition, undergo analyte-dependent conformational changes, opening a wealth of possible signal transduction schemes that allow to study the kinetic and thermodynamic details of their interactions with the target molecules, and provide highly-sensitive quantification of the same [4-7].

In the design of new aptamers, the development of non-canonical protocols for the generation of structural diversity (i.e., not based on the iterative variation of their sequence) is a subject of great interest. For example, the use of synthetic nucleic acids could lead to the development of improved aptamers by modification of their original chemical identity. Post-selection techniques are normally used in this field, in which DNA or RNA hits that are provided by Systemic Evolution of Ligands by Exponential Enrichment (SELEX) or similar techniques are replaced with analogues of the nucleic acid structure to increase affinity, stability, and resistance to degradation [8]. Substitution with a variety of other structures, such as locked nucleic acid (LNA),[9] unlocked nucleic acid (UNA) [10], L-RNA based Spiegelmers [11], expanded genetic alphabet [12, 13] and functional group bearing nucleobases [14] has proved to be successful. A crucial point in these 'substitution' approaches is how far a DNA aptamer structure can be varied without losing, or even improving, their essential interactions with the target molecule. The aptamer ligand interaction is dictated not only by the secondary structure, but also by the specific non-covalent interactions that the nucleic acid is capable to install with the target. This is guided by the electrostatic interactions, but other types of interactions such as cooperative hydrogen bonding, stacking interactions and hydrophobic effects can play important roles. In some cases, the overwhelming role of electrostatics can result in a strong dependence of the interactions on environmental factors such as ionic strength or pH. In the design of possible alternative aptamer structures, it would be interesting to understand if the proper disposition of functional groups in a DNA aptamer can be effective also in the case of drastically different derivatives lacking electrostatic interactions. Indeed, it has been shown that neutral-backbone, isostructural alkylphosphonate oligonucleotides can be selected as aptamers for streptavidin using an autonomous selection process based on DNA polymerase engineering [15].

The oligonucleotide analogues which represent one of the farthest models from nucleic acid original structures is that of Peptide Nucleic Acids (PNAs) [16]. PNAs are synthetic DNA

analogues in which a neutral peptide-like backbone composed of repeated N-(2-aminoethyl) glycine units substitutes the sugar-phosphate backbone of the natural nucleic acids (**Figure 1)**. These compounds exhibit high affinity and high selectivity in binding complementary DNA and RNA. The neutral charge of the backbone provides high thermal stability to PNA complexes in solution with interactions barely affected by variations in solution composition such as pH and ionic strength. Most importantly, PNAs are very stable from a chemical or a biological point of view and are not degraded by peptidases or nucleases commonly present in biological fluids. Thus, many PNA-based RNA or DNA ultrasensitive detection biosensors for early disease diagnoses have been developed [17-22], including gFET sensors [19]. The higher sensitivity using PNA strands in DNA analysis is linked to their neutral backbone, which eliminates electrostatic repulsions between the two hybridised strands and reduces the background noise. SELEX iterative methods are not possible for PNAs, so these compounds are eventually suitable only for the "post-SELEX" approach [23, 24]. It would be very useful to study the difference between a DNA and a PNA aptamer bearing the same nucleobase sequence and to understand under which conditions PNA can actually mimic high affinity DNA aptamers. The replacement of DNA with a PNA would result in a substitution of the negatively charged phosphate groups of the former with the neutral backbone of the latter, while keeping intact the possibility of achieving the same interactions mediated by the nucleobases. One great advantage of using PNAs as aptamers over DNA aptamers would be their well-known intrinsic resistance to both peptidases and nucleases [25, 26], which is due to their "unnatural" structure, and which makes them very persistent when exposed to biological fluids or hydrolytic enzymes.

In this paper, we follow up on recent work we performed using a DNA aptamer to detect selectively cTnI *via* a gFET sensor [27]. Graphene-based field-effect transistors (gFET) have been proven to be ideally-suited for the sensitive detection of various biomarkers and to reliably study their interaction with surface-immobilized DNA aptamers [28-31] with electrolyte-gated gFET sensors in combination with DNA-aptamers are a preferable choice, since their compact structure enables target capturing within the Debye length limitation [2, 32]. While PNA aptamers have been proposed in the past as DNA aptamer analogues in solution hybridization studies, no previous work reported gFETs and PNA aptamers for protein sensing and study of PNA-protein interactions. Although the possibility to have selective PNA aptamers for metal ions [33] and proteins [34-36] has been shown in the past and sequence selective PNA-protein interactions have been reported [37], this work is the first example of a PNA aptamer able to interact with a specific protein in the picomolar range. Indeed, we show that by choosing the

proper target, a PNA aptamer gFET sensor, in combination with a stable covalently modified graphene surface, can sense PNA/protein interactions in a similar manner as a DNA aptamer transducer.

2. Results and Discussion

2.1. Specific-PNA aptamer probe synthesis and characterisation

A PNA aptamer with the same sequence as the well-known HD1 thrombin DNA aptamer was previously reported to sense its target by fluorescence 'switch on [24]. Follow up studies based on Micellar Electrokinetic Chromatography suggested that the affinity of this probe might be lower than that of DNA, and non-specific to the target protein [38]. Since the DNA aptamer interaction with thrombin was found to be sensitive to ionic strength, we reasoned that the electrostatic component was decisive and this model was not optimal for developing an efficient PNA aptamer, as confirmed also by interaction data obtained by us using fluorescence anisotropy and surface plasmon resonance measurements (**Figures S1 and S2**).

We focused consequently on a different aptamer sequence for the synthesis of a cTnI PNA aptamer (**Figure 1**), showing the following characteristics: a) a high affinity for target, and b) a less dramatic dependence of the interaction upon ionic strength variation. The ideal choice was found in a DNA-based aptamer which binds with high affinity to cTnI. A single-stranded DNA aptamer against cTnI, called Tro4 aptamer, was identified by Jo Hunho in 2015 [39], with a reported dissociation constant, i.e. a half saturation-constant, K_D=270 pM. When used as a bioreceptor in an electrochemical sensor, a detection limit of 1.0 pM (24 pg mL^{-1}) was reached. Some of us had determined a K_D=2.1 pM for the electrons' regime using a gFET modified with the same aptamer using "click" chemistry [30], while a K_D=6.6 pM was extracted from a related electrochemical interface [40].

To allow for the direct comparison of the performance with our previously-developed DNA-based gFET [30], a PNA aptamer with a pending azido function at the 5' end was synthesised in order to be immobilized onto the graphene transducer channel via a click chemistry approach (**Figure 1**) [41].

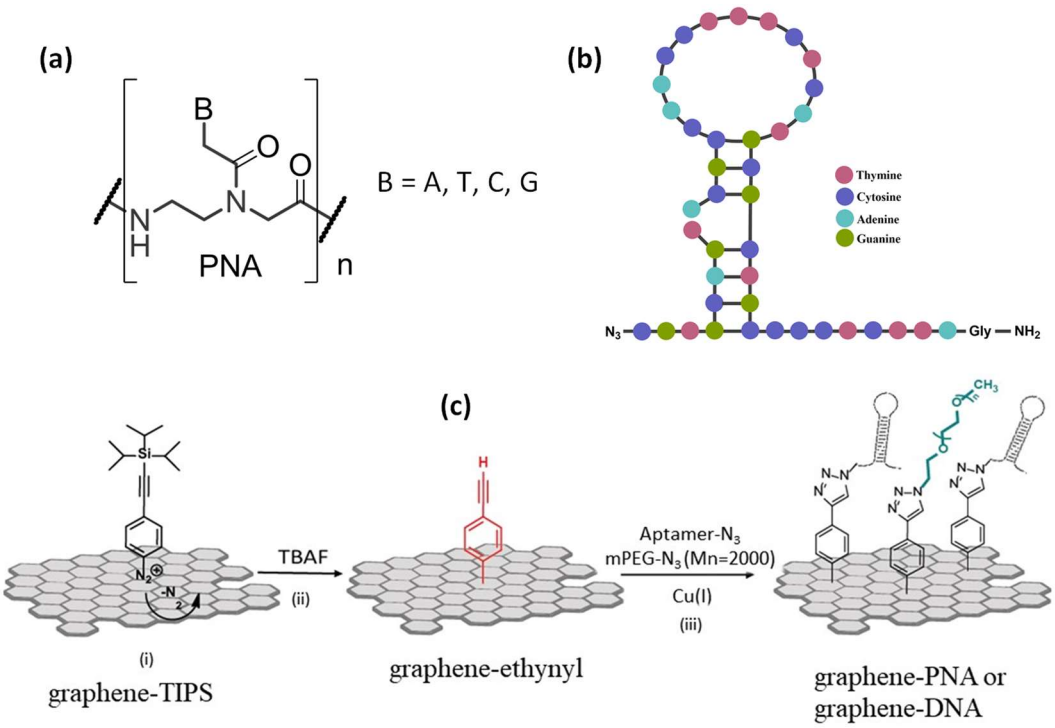

Figure 1: DNA or PNA aptamer modified graphene-based field effect transistors for cardiac troponin I (cTnI) sensing: (a) Schematic structure of cTnI PNA aptamer; (b) structure of PNA aptamer probe (same sequence for DNA); (c) graphene functionalization: (i) electrochemically driven anchoring of 4-[(triisopropylsilyl)ethynyl]benzene diazonium tetrafluoroborate (TIPS-Eth-ArN_2^+) onto graphene forming graphene-TIPS, followed by (ii) chemical deprotection of the triisopropylsilyl function with tetrabutylammonium fluoride (TBAF) giving a graphene-ethynyl to which (iii) azide-terminated bioreceptors were covalently linked using Cu(I) catalyzed "click" chemistry.

The synthesis of the cTnI-specific PNA aptamer was performed according to solid-phase protocols using Boc-chemistry that allows higher yields for very long sequences such as that of the troponin aptamer (40 bases long). Since functionalization with azido groups on resin is difficult due to the use of harsh acidic conditions for cleavage from the solid support, the PNA was first removed from the resin, reacted with N-succinimidyl ester of 2-azidoacetic acid and finally purified by HPLC purification to provide azide-PNA conjugate (**Figure 2a**). Long PNA aptamers have generally poor aqueous solubility and a tendency to aggregate. This was overcome by using PNA aptamer stock solutions of 100 µM in a mixture of water:acetonitrile (8/2).

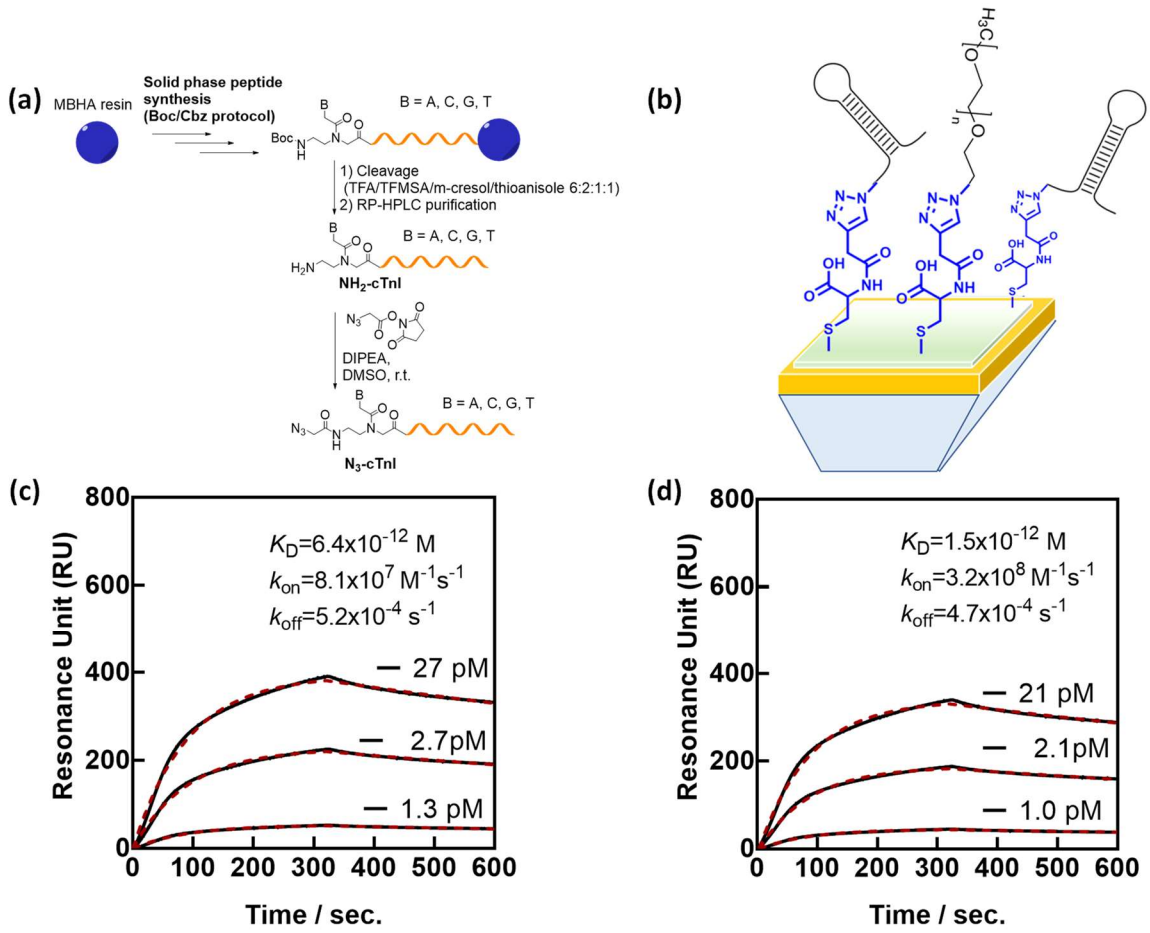

Figure 2: **PNA synthesis and affinity characterisation**: (a) Synthetic steps used for obtaining the azido-PNA aptamer N_3-cTnI. (b) Schematic diagram of the plasmonic sensor modified with N_3-PNA aptamer. (c) SPR sensograms measuring the apparent binding affinity of cTnI (1.3, 2.7 and 27 pM) to the surface-immobilized N_3-DNA. The SPR binding curves were recorded with a Biacore (T200) using 1× PBS (pH 7.4). (d) SPR sensograms measuring the apparent binding affinity of cTnI (1.0, 2.1, 21 pM) to surface-immobilized N_3-PNA. The interaction with cTnI was recorded at a flow rate of 30 µL min^{-1}. The 1:1 Langmuir binding fits are the dashed red lines.

The binding affinities of the DNA and PNA aptamers were determined using surface plasmon resonance (SPR). To operate under comparable conditions as on the gFET, the N_3-DNA and N_3-PNA aptamers were clicked to a 4-pentynoyl-cysteine modified gold prism (**Figure 2b**) and the interaction with cTnI was sensed. A dissociation constant K_D=6.4 pM with k_{on} = 8.1×10^7 M^{-1} s^{-1} and k_{off} = 5.2×10^{-4} s^{-1} was determined for the DNA aptamer (**Figure 2c**) and compared to N_3-PNA linked to gold SPR chips. From the SPR sensograms in **Figure 2d**, K_D=1.5 pM, with k_{on} = 3.2×10^8 M^{-1} s^{-1} and k_{off} = 4.7×10^{-4} s^{-1} were determined. The affinity for cTnI is clearly

preserved in the PNA case (**Table 1)**. PNA probes showed general larger k_{on} values with comparable k_{off} rates. Interestingly, the affinity remained comparable over a wide pH range, while the DNA aptamer showed increased affinity at more acid as well as more basic medium. This indicates that the PNA aptamer is more robust to pH variations

Table 1: SPR data recorded on a CM5 chip (Biacore T200) on DNA- and PNA-modified gold chips at different pH values (1× PBS and pH adjusted with HCl or NaOH addition) and at different ionic strengths (0.01-1× PBS).

Conditions	DNA aptamer			PNA aptamer		
	K_D / pM	$k_{on}\times10^7$/ M^{-1} s^{-1}	$k_{off}\times10^{-4}$/ s^{-1}	K_D / pM	$k_{on}\times10^7$/ M^{-1} s^{-1}	$k_{off}\times10^{-4}$/ s^{-1}
pH 7.4 1 × PBS	6.4±0.9	8.1±1.3	5.2±0.4	1.5±1.1	32.0±1.2	4.7±0.9
pH 7.4 0.1 × PBS	7.7±0.9	7.9 ±1.1	6.1±0.6	1.6±1.4	30.0±3.2	4.9±0.6
pH 7.4 0.01 × PBS	7.3±1.1	8.0±1.7	5.9±0.5	1.3±1.1	30.6±2.1	3.9±0.1
pH 4.0 1 × PBS	15.0±0.5	1.3±0.8	2,0±0.2	1.1±1.1	34.0±2.0	3.8±0.2
pH 9.0 1 × PBS	23.3±0.5	1.8±0.8	4,2±0.2	1.3±1.5	19.0±3.5	2.5±0.3

2.2. PNA- and DNA-modified gFET sensors

As in our previous work using N_3-DNA aptamer [30], the gFET design is based on the transfer of CVD-grown graphene onto interdigitated gold electrodes (IDE) consisting of 90 electrode pairs of 10 µm in width with a 10 µm separation and total surface area of 3.6 mm^2. For cTnI specific interactions, graphene was covalently modified with the cTnI -specific azido-PNA aptamer (**Figure 1b**) in a three-step process based on electrochemical reduction of 4-[(triisopropylsilyl)ethynyl]benzenediazonium tetrafluoroborate (TIPS-Eth-ArN_2^+) forming graphene-TIPS, followed by chemical deprotection of the triisopropylsilyl (TIPS) function to provide graphene-ethynyl and subsequent covalent integration of the bioreceptors using Cu(I) catalysed "click" chemistry, resulting in graphene-PNA. **Figure 3a** shows the Raman spectra of initial graphene and graphene-PNA presenting three prominent bands at 1350 cm^{-1} (D band – defects in the graphene sheet), 1580 cm^{-1} (G band – sp^2-carbon), and 2700 cm^{-1} (2D band, also called G′ – secondary D-band) [42]. The position of the G band is dependent on the number of layers and can be used to estimate the graphene thickness. In our case, the G band of graphene is around 1585.1±2.3 cm^{-1} with the deviation error being ascribed to local changes in graphene thickness: downshift to ≈1581 cm^{-1} indicates few-layer graphene, while upshift to ≈1587 cm^{-1} is consistent with monolayer graphene. We estimated I_{2D}/I_G=1.53±0.05 for graphene, 0.61±0.03

for graphene-TIPS, 0.99±0.03 for graphene-ethynyl and 0.86±0.12 for graphene-PNA. The I_D/I_G ratio changed from 0.11±0.02 for graphene to 0.59±0.17 for graphene-TIPS and 2.35±0.14 for graphene-ethynyl, indicating an increase of graphene disorder as expected. Clicking of the PNA aptamer to graphene-ethynyl results in I_D/I_G=2.43±0.41, indicating no further increase of disorder, also visible by the maintenance of the D peak intensity (inset **Figure 3a)**.

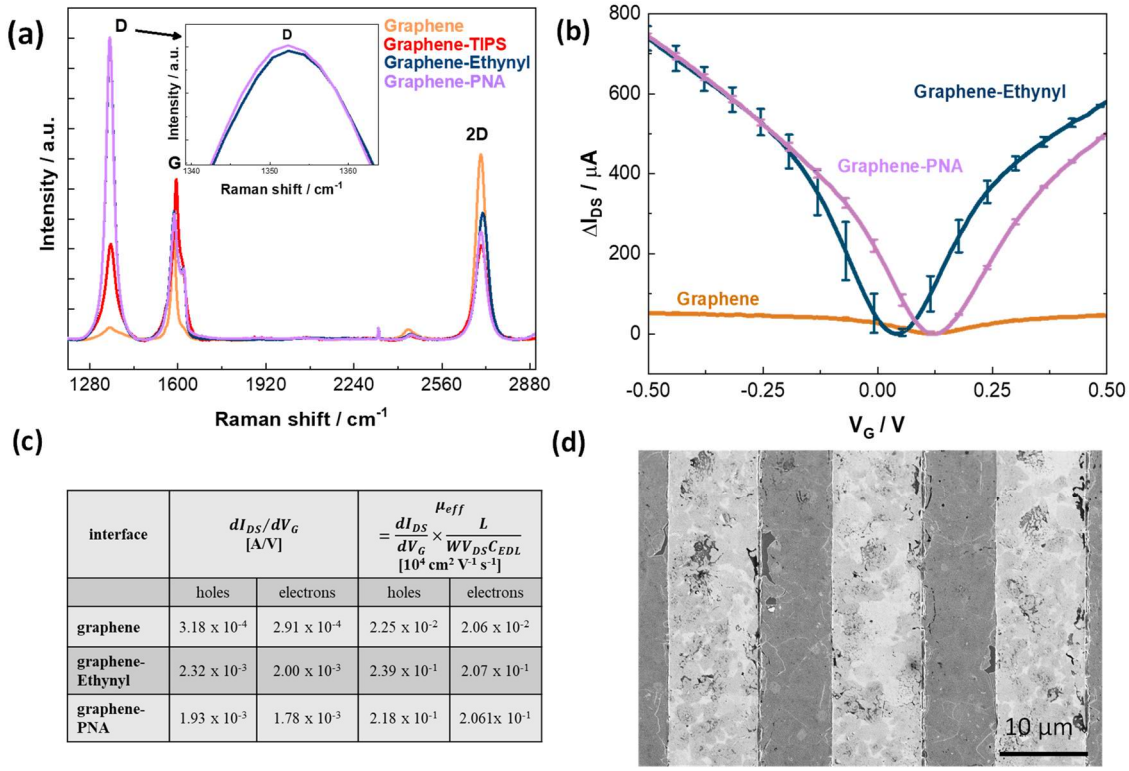

interface	dI_{DS}/dV_G [A/V]		$\mu_{eff} = \frac{dI_{DS}}{dV_G} \times \frac{L}{WV_{DS}C_{EDL}}$ [10^4 cm^2 V^{-1} s^{-1}]	
	holes	electrons	holes	electrons
graphene	3.18 x 10^{-4}	2.91 x 10^{-4}	2.25 x 10^{-2}	2.06 x 10^{-2}
graphene-Ethynyl	2.32 x 10^{-3}	2.00 x 10^{-3}	2.39 x 10^{-1}	2.07 x 10^{-1}
graphene-PNA	1.93 x 10^{-3}	1.78 x 10^{-3}	2.18 x 10^{-1}	2.061x 10^{-1}

Figure 3: Characterisation of the graphene-PNA based FET. (a) Raman spectra of initial graphene (orange), graphene-TIPS (red), graphene-ethynyl (dark blue) and graphene-PNA (purple). (b) dc characteristics ΔI_{DS}-V_G of gFET for V_{DS}=50mV, recorded after each functionalization step, with ΔI_{DS} = I_{DS}-minimum (I_{DS}). See **Figure S3** for raw data and leakage current taken from each step. (c) Table of the anodic hole mobility, μ_h, and the cathodic electron mobility, μ_e, as determined from **Figure 3c**. See **Figure S4** for C_{EDL} calculations used for extraction of mobility. (d) SEM image of PNA-modified graphene (**Figure S5** for SEM images recorded after each modification step).

Graphene functionalization was in addition monitored through changes in transfer characteristics. Upon grafting the diazonium, a constant shift of the V_{Dirac} to higher gate voltages (≈0.2 V), was observed and a shift to approximately the initial values (for bare graphene) once the triisopropylsilyl (TIPS) group is chemically removed (**Figure 3b**). Previously [30], we had found an initial Dirac point at around 0.3 V for unmodified graphene,

whereas in this work a lower value of around 0.1 V was noted. This difference is due to the transfer process – graphene preparation after growth, water/ammonium persulfate and copper contaminations, and manual handling.

A drastic increase in the mobilities of holes and electrons after the electrochemical grafting of TIPS-Eth-ArN_2^+ onto graphene is observed, remaining stable with deprotection of the TIPS function. To this interface PNA-aptamers as well as poly(ethylene glycol) (PEG) in a ratio of PNA/PEG=2/1 were linked. The addition of a PEG units aims at the prevention of non-specific interactions and serves as anti-fouling agent; it also increases the Debye length due to a decrease of the dielectric constant of the electrolyte as reported previously [30]. Once the Debye length increases, the sensitivity the device increases consequently, since the charges previously residing beyond this length are no longer screened. Addition of the PNA aptamer together with poly(ethylene glycol) (PEG) in a ratio of PNA/PEG=2/1, revealed a shift of the Dirac point to more positive gate voltages, indicative of device n-doping. Considering that PNA is not charged, the shift in the Dirac point cannot be attributed to the formation of a charged monolayer, but rather to combined effects such as modification of local dielectric constant and/or association of the layer with ions through dipolar and hydrogen bonding interactions. In a control experiment, graphene was only modified with PEG units (**Figure S6**) revealing an identical positive shift compared to graphene modified with PNA/PEG. The n-doping effect is consequently not attributed to the PNA-aptamer .

As shown previously, charge mobilities increase dramatically after TIPS modification (**Figure 3c)**. The anodic hole mobility, μ_h, and cathodic electron mobility, μ_e, were obtained (Table of **Figure 3d**) from the anodic and cathodic linear slopes of the $I_{DS}V_{GS}$ plots using equation μ_e or $\mu_h = \frac{dI_{DS}}{dV_G} \times \frac{L}{WV_{DS}C_{EDL}}$ with L and W being the channel length and width (1.00×10^{-5} m and 4.90×10^{-1} m, respectively), V_{DS} is the source–drain voltage (V_{DS} = 50 mV), and C_{EDL} the electrical double layer capacitance extracted from the leakage current (C_{EDL}=5.76 μF cm^{-2} for unmodified graphene, C_{EDL}=3.95 μF cm^{-2} for ethynyl-modified graphene and C_{EDL}=3.61 μF cm^{-2} for PNA-modified graphene). The values of capacitances used to calculate the mobility of charge carriers were extrapolated from fitting the leakage current at different scan rates recorded at different applied gate voltages (**Figure S3**). Moreover, the leakage current was recorded in all measurements to ensure that the processes occurring in the vicinity of the channel's surface is mainly (desirably, only) due to the formation of an aptamer-protein complex instead of parallel electrochemical reactions. Leakage currents are currents between the device and the electrolyte under V_G bias and highly undesirable as they are interfering with

the current of interest (source-drain current in this case). It was demonstrated previously [43] that leakage currents at the gate electrode are products of faradaic and capacitive reactions occurring at the surface, a possibly outcome of oxygen reduction reactions. Considering that these parasitic currents might be a product of graphene's oxygen-containing groups/defects, they are transistor specific and need to be determined.

The SEM image on **Figure 3d** of the PNA modified graphene, indicates a complete coverage of the drain-source channel in addition to graphene's preservation. **Figure S5** shows SEM images of the previous functionalization steps, where the introduction of small defects along each step is observed, although preserving the overall surface of graphene. In general, SEM revealed the good quality of graphene placed on top of the interdigitated electrodes, with low density of defects despite some evident holes and perturbations, with a few wrinkles, folds and nucleation points that are typically present on graphene samples. Moreover, the presence of the Au interdigitated electrodes (lighter stripes) adds a height different between glass and Au, potentiating graphene ruptures on the Au edges.

2.3. PNA-based gFET for cardiac troponin I detection

Figure 4a depicts the transfer characteristics of the PNA-modified gFET during exposure to cTnI of increasing concentrations in 0.01× PBS (pH 7.4) after 10 min stabilization for each concentration. No change in the shape of the ΔI_{DS}-V_{GS} curves were observed besides a cathodic shift of the Dirac point (**Figure 4a**) and a positive (**Figure 4b**) and a negative shift (**Figure 4c**) of the I_{DS} in the electron and hole regimes, respectively. At this physiological pH, the positively charged cTnI analyte induces a negative charge in the graphene channel, generating more electrons, making them the majority carriers. By performing a linear fit to the measurement data in the regime (3 - 60 pg mL^{-1}), the sensitivity of the gFET, defined as $\Delta I_{DS}/\Delta C_{cTnI}$, was determined to be 2.12 ± 0.57 μA/pg mL^{-1}. This sensitivity, along with the estimated noise level of 4.21 μA for the measurement system, was used to determine the theoretical limit of detection (LoD) with LoD = (S/N × Noise)/Sensitivity being equal to 6.0 ± 1.0 pg mL^{-1} (S/N = 3). These results are comparable to that obtained for the DNA aptamer sensor with a LoD =3.3 ± 0.7 pg mL^{-1} (S/N = 3) [30]. Using **Figure 4d**, a limit of quantification LoQ of 13.2 ± 1.0 pg mL^{-1} was extracted with a dynamic response of the gFET covering the concentration range relevant for patient diagnostic with cTnI critical levels (25 pg mL^{-1} – 50 pg mL^{-1}).

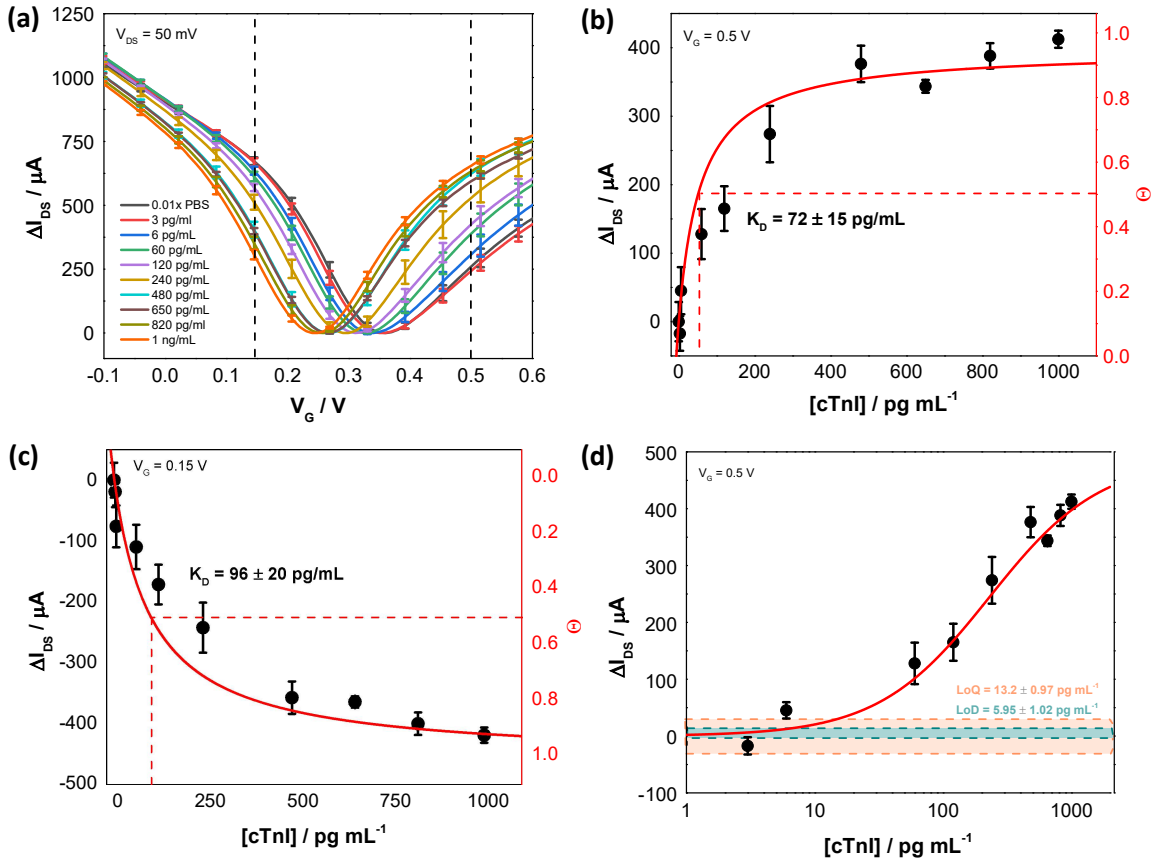

Figure 4: **PNA aptamer-based gFET sensing of cTnI in 0.01× PBS**. (a) Transfer characteristics of graphene-PNA after 10 min stabilization for each cTnI concentration (3, 6, 60, 120, 240, 480, 650, 820 and 1000 pg mL^{-1}) in 0.01× PBS (pH 7.4) without washing steps, applied V_{DS} = 50 mV. The current values were treated to start at zero using the equation ΔI_{DS} = I_{DS}-minimum (I_{DS}). Dotted black lines represent the V_G values in which the current was monitored for each cTnI concentration (**Figure S7** for raw data and leakage current). (b) Change of ΔI_{DS} as a function of cTnI concentration at a fixed gate voltage V_G = 0.5 V with respective Langmuir binding isotherm. (c) Change of ΔI_{DS} as a function of cTnI concentration at a fixed gate voltage V_G = 0.150 mV with respective Langmuir binding isotherm. (d) Change of ΔI_{DS} with log of cTnI concentration at a fixed gate voltage V_G = 0.5 V, showing the values of LoD and LoQ.

When using the Langmuir isotherm format in equation (1),

$$\boldsymbol{\Theta = \frac{I_{DS}(C_0)}{I_{DS}(C_\infty)} = \frac{K_D \times C_0}{1 + K_D \times C_0}} \qquad (1)$$

with K_D being the dissociation constant in which half of the receptor's binding sites are occupied in the system in equilibrium, C_0 and C_∞ are respectively the cTnI initial and infinite bulk concentrations correlating to $I_{DS}(c_0)$ and $I_{DS}(c_\infty)$ being the drain-source current at the respective cTnI concentrations. Assuming a 1:1 complex, $K_D = 72 \pm 15$ pg mL^{-1} (3.0 ± 0.6 pM) for the electrons' regime and $K_D = 96 \pm 20$ pg mL^{-1} (4.0 ± 0.8 pM) for the holes' regime were calculated by fitting the data in **Figure 4b** and **4c**, respectively. The results are comparable to that of DNA aptamers with $K_D = 51 \pm 9$ pg mL^{-1} for DNA [30].

The PNA proved to be specific to cTnI, validated by recording the current changes using another cardiovascular biomarker, BNP-32 as well as bovine serum albumin (BSA) and thrombin, an unique molecule that functions both as a procoagulant and anticoagulant (**Figure 5**). In contrast to the DNA-aptamer gFET, where a decrease in current was observed for BNP-32 although having almost an identical isoelectric point as cTnI [30], no current change was recorded for the PNA-aptamer-based gFET in the presence of BNP-32 at $V_G = 0.5$ V. Thrombin, with an isoelectric point between 6.3-7.6 and being almost neutral at pH 7.2 as well as BSA with an isoelectric point between 4.5–4.8 and being negatively charged, show both a decrease in current a low analyte concentration, which is preserved in the case of BSA at higher concentrations, while the current is somehow increasing for thrombin with a final value comparable to that of BNP-32, indicating excellent selectively for cTnI. By integration of a cTnI non-specific PNA aptamer (N_3-CH_2CO-AEEA-GGTTGGTGTGGTTGG-Gly-NH_2, N_3-ND1-PNA) with azido moiety, we could show in addition that no bind to cTnI occurred in this case (**Figure 5d**).

The reproducibility of the electrode fabrication was determined on 5 devices and the long-term stability of the sensor showed a loss of 2.3% when tested in cTnI (100 pg mL^{-1}) upon storage of the electrode at 4°C for a month. The sensor could be regenerated by immersion into NaOH (0.1 M, pH 12.0) for 20 min. The PNA aptamer sensor performed in very similar way to the DNA homolog in the recognition of cTnI, with similar, though not identical, K_D. This, in turn, implies that, surprisingly, comparable interactions can occur both with the negatively charged DNA and with the neutral PNA aptamers, suggesting a major role of hydrogen bonding, dipolar and stacking interactions in the recognition process. The similarity in DNA and PNA affinity and selectivity towards cTnI might be due to the occurrence of similar secondary structures; namely, the DNA hairpin structure proposed for the cTnI aptamer might be formed also in the PNA analogy, reinforced by the stronger PNA:PNA interactions. The formation of the stem in the secondary structure should be less dependent on ionic strength, unlike DNA aptamers for

which an increase in the ionic strength should increase the stem stability. The main advantage of the use of a PNA-aptamer in sensing seems consequently linked to known higher chemical stability and lack of enzymatic degradation.

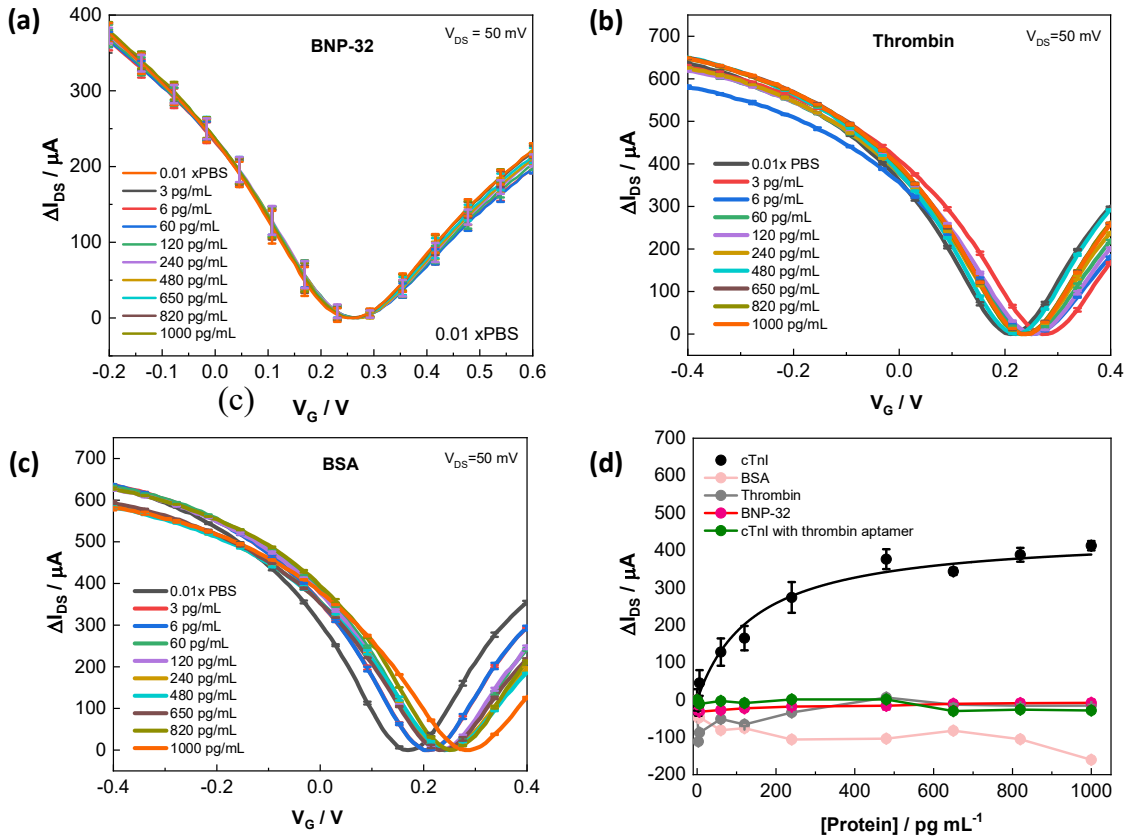

Figure 5: **Selectivity of PNA sensor to cTnI in 0.01× PBS**: (a) Transfer characteristics of graphene-PNA after stabilization for each (a) BNP-32, (b) Thrombin, and (c) BSA concentrations (3, 6, 60, 120, 240, 480, 650, and 820 pg mL^{-1}) in 0.01× PBS (pH 7.4) without washing steps, with applied V_{DS} = 50 mV. The current values were treated to start at zero using the equation $\Delta I_{DS} = I_{DS}$-minimum(I_{DS}) (**Figure S8** for raw data and leakage current). (d) Change in ΔI_{DS} for increasing concentrations of cTnI (black, same as **Figure 4b**) BNP-32 (red), thrombin (grey), BSA (pink), on cTnI specific PNA surface as well as cTNI on thrombin PNA aptamer suface at a fixed gate voltage V_G=0.5 V.

2.4. PNA-aptamer gFET performance in solutions of different ionic strengths and pH

The replacement of the DNA aptamer by a PNA aptamer does not result in a significantly different sensing behaviour in all solutions studied, even at a variation of the ionic strength of the analyte solution of more than 2 orders of magnitude and a variation of its pH from 4 to 9. This is shown in **Figures 6a, c,** respectively, for the variation of ionic strength and in **Figures**

6b, d for the pH variation. In case of ionic strength variation, the PNA aptamer showed nearly identical affinities, whereas the K_D values of the DNA aptamers measured under the same (extreme variations of the analyte) conditions (**Figure S9**) showed a change of K_D of less than a factor of 3 (despite the significant variation of the ionic milieu of the analyte solutions. Similar behaviour was recorded in solutions of different pH but constant ionic strength (**Figures 6 b, d, Figure S9,** respectively).

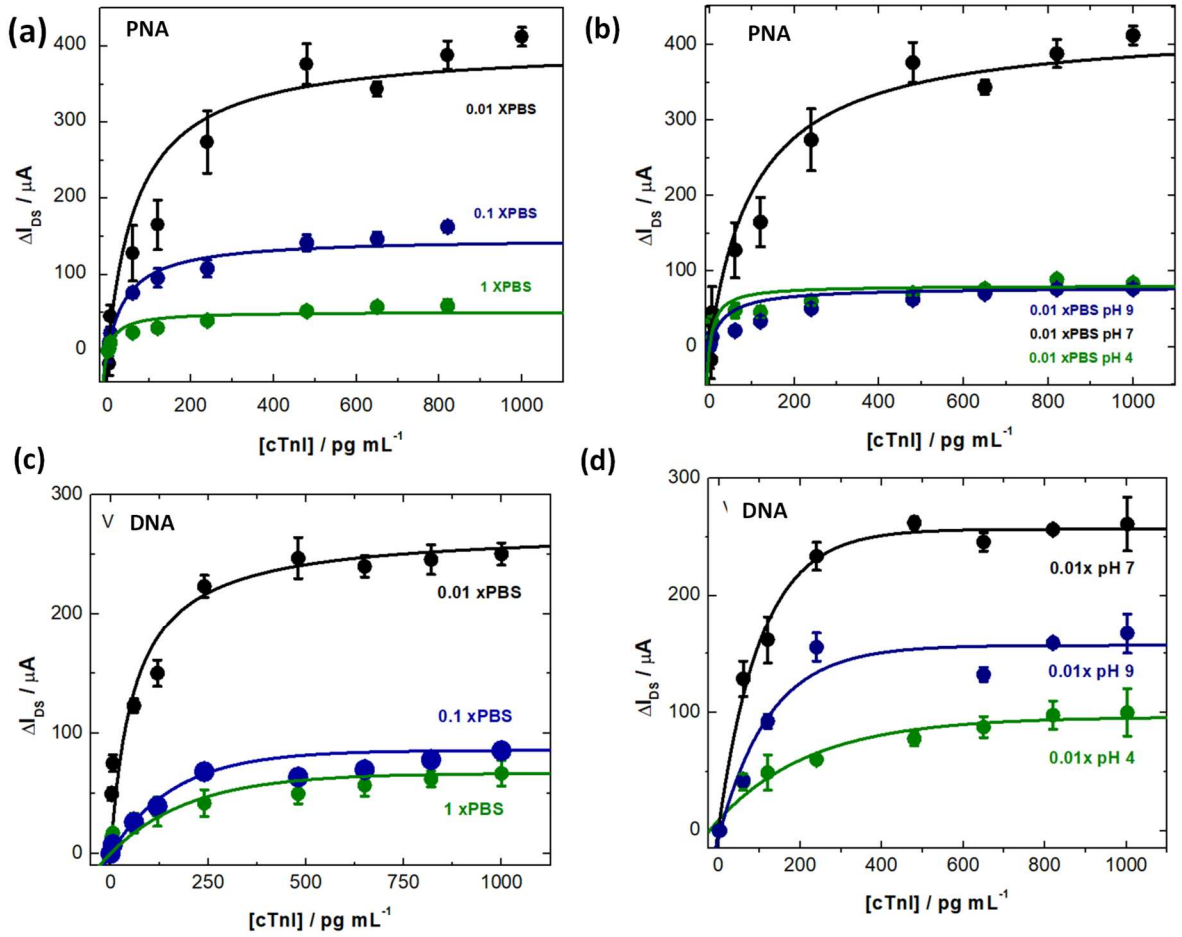

Figure 6: **Ionic Strength and pH effects of DNA and PNA modified gFET**: (a) Change of ΔI_{DS} on graphene-PNA for each cTnI concentration at a fixed gate voltage V_G = 500 mV with respective Langmuir binding isotherm for 0.01, 0.1 and 1× PBS solutions. (**Figure S10** raw data and leakage current). (b) Change of ΔI_{DS} in graphene-PNA for each cTnI concentration at a fixed gate voltage V_G = 500 mV with respective Langmuir binding isotherm for pH 4, 7 and 9 in 0.01× PBS solutions (**Figure S11** raw data and leakage current). (c) Change of ΔI_{DS} on graphene-DNA for each cTnI concentration at a fixed gate voltage V_G = 500 mV with respective Langmuir binding isotherm for 0.01, 0.1 and 1× PBS solutions. (d) Change of ΔI_{DS} on graphene-DNA for each cTnI concentration at a fixed gate voltage V_G = 500 mV with respective

Langmuir binding isotherm for pH 4, 7 and 9 in 0.01× PBS solutions. (**Figure S9** for surface coverage plots as a function of cTnI concentrations).

This concludes that for the DNA aptamer, binding affinities depend both on the ionic strength and the pH of the medium, although only weakly, with K_D increasing with increasing ionic strength and pH. The pH and ionic strength dependence of the signals imply a careful control of these two parameters when measuring in real samples, which can be obtained by dilution, desalting and pH adjustment. This is in contrast to the PNA aptamer where the K_D values remained comparable under all experimental conditions (**Table S1**). Though the PNA aptamer has not a dramatically higher affinity for cTnI, it does help in reducing the influence of these parameters, showing more stable and consistent K_D values, thus allowing more adaptability to different conditions in the sample matrices. It is also important to consider that unmodified gFETs depend strongly on ionic strength and solution pH (**Figure S12**). In the case of unmodified gFET, the pH dependency is believed to be due to hydroxyl and carbonyl groups present on graphene's surface. There seems to be no evident pH dependency of our transistors after fabrication, perhaps indicating the good overall surface quality.

Conclusion

In conclusion, this work demonstrated, for the first time, the application of a PNA aptamer specific to cTnI as a bioreceptor in gFETs with picomolar range affinity. In contrast to DNA aptamers, PNA aptamers carry no charge they are expected to be the better choice for electrical transducers, based on change in surface charges. The superiority of PNA-aptamer gFET sensing over DNA-aptamer one in terms of assay sensitivity as limited with a respective limit of detections of 3.34 ± 0.69 pg mL^{-1} (DNA-aptamer) and 5.95 ± 1.02 pg mL^{-1} (PNA aptamer). The similarity in DNA and PNA affinity towards cTnI might be due to similar secondary structures. The PNA-based transducer proved however to be insensitive to changes in pH and ionic strength with dissociation constants variations are in the error of the experiment. This differs from the DNA aptamer case, for which slight changes in K_D values were found when changing the ionic and pH properties of the sensing medium. The neglectable pH and ionic strength dependency upon PNA-aptamer/cTnI interaction is a further confirmation that electrostatic interactions are not prevalent. Since both DNA and PNA share the same nucleobases, the nucleobase-protein interactions are considered the most important origin of the observed

affinities and selectivity. Indeed, hydrogen bonding, dipolar and stacking interactions seem to play a major role in the recognition process observed. Since PNAs have many applications in diagnostics and therapeutics, the present results form the base of envisaging PNA scaffold for study of other PNA/protein interactions. The understanding of PNA derived affinity and specificity compared to DNA aptamers can in the long run lead to a better understanding of their behaviour in biological environments. The combination with sensing technology such as gFET transducer can lead to very robust and high-performance sensor devices.

Acknowledgement

Financial supports from the Centre National de la Recherche Scientifique (CNRS), the University of Lille are acknowledged. This work has benefited from the equipment and framework of the COMP-HUB Initiative, funded by the 'Departments of Excellence' program of the Italian Ministry for University and Research (MUR, 2018-2022) for the Department of Chemistry, Life Sciences and Environmental Sustainability of the University of Parma. The TeachInParma Program is also acknowledged for sponsoring supervision and collaborative work of WK at the University of Parma premises.

3. Experimental Section

Materials: The Boc-protected PNA monomers were purchased from ASM Research Chemicals GmbH (Hannover, Germany). Thrombin, purified from human plasma, was purchased from EUROCLONE S.P.A. (Milano, Italy). 5(6)-Carboxy-tetramethylrhodamine (TAMRA) was purchased from Novabiochem (Darmstadt, Germany). O-(Benzotriazol-1-yl)-N,N,N',N'-tetramethyluronium hexafluorophosphate (HBTU) was purchased from Fluorochem Ltd (Derbyshire, United Kingdom). *N,N*-diisopropylethylamine (DIPEA) was procured from Alfa Aesar (Kandel, Germany). Piperidine, GPR RECTAPUR, was obtained from VWR International srl (Milano, Italy). N,N'-diisopropylcarbodiimide (DIC) and 3,4-dihydro-3-hydroxy-4-oxo-1,2,3-benzotriazine (DhBtOH) were purchased from TCI chemicals. Dichloromethane (DCM), N,N-Dimethylformamide (DMF), acetonitrile were purchased from Carlo Erba reagents (Milano, Italy). Rink amide-MBHA resin LL (100-200 mesh) was purchased from Novabiochem. Biotin, Boc-Gly-OH, Trifluoroacetic acid (TFA), formic acid (FA), trifluoromethanesulfonic acid (TFMSA), azidoacetic acid, *N*-hydroxysuvvinimide (NHS), pyridine, thioanisole, *m*-cresol, acetic anhydride, diethyl ether, phosphate buffer tablets

(PBS, 0.1 M), *N*-butyl hexafluorophosphate, tetrabutylammonium fluoride (TBAF), copper(II) sulfate ($CuSO_4$), L-ascorbic acid, ethylenediaminetetraacetic acid (EDTA), and methoxypolyethylene glycol azide PEG (mPEG-N_3, average Mn=2.000) were obtained from Sigma-Aldrich and used as received. 4-((trisopropylsilyl)ethynyl)benzenediazonium tetrafluoroborate (TIPS-Eth-ArN_2^+) and succinimidyl 2-azidoacetate (see paragraph **S1**) were synthesized as reported previously.[38, 44] The 5'-azide modified troponin I DNA aptamer (5'-N_3-TTT-TTT-CGT GCA GTA CGC CAA CCT TTC TCA TGC GCT GCC CCT CTT A-3') was procured from integrated DNA Technologies (Leuven, Belgium). The unspecific aptamer was a 5'-azide modified Brain Natriuretic Peptide-32 aptamer (5′-N_3-TTT-TTT-GGC GAT TCG TGA TCT CTGCTC TCG GTT TCG CGT TCG TTC G-3′) and was purchased from IDT Technologies (Leuven, Belgium).

Recombinant human cardiac troponin I protein (MW=24 kDa) was obtained from Abcam (Cambridge, UK). BNP-32 peptide (MW = 3.4 kDa) was obtained from BACHEM AG (Switzerland). Graphene is synthesized in-house as described in Ref.[30] and interdigitated microelectrodes (ED-IDE1-Au w/o SU8) are provided by Micrux Technologies. Thrombin from human plasa mas purchased from MercK. Bovin serum albumin (BSA) was obtained from Sigma-Aldrich

cTnI PNA Aptamer synthesis. NH_2-cTnI PNA, the amino precursor of the tested PNA-aptamer, was synthesized according to manual solid phase synthesis on MBHA resin, loaded with Boc-Gly-OH (0.20 mmol/g) in 5 μmol scale. The following solutions were used: a) Boc deprotection: TFA/*m*-cresol 95/5; b) Capping: acetic anhydride/pyridine/dry DMF 1/25/25; c) piperidine wash: 10% piperidine in DMF; d) Cleavage: TFA/TFMSA/*m*-cresol/thioanisole 6/2/1/1. The PNA monomers were attached according to standard Boc/Cbz protocols, consisting in: 1) deprotection 2 × 4 min; 2) DCM wash; 3) DMF wash; 4) Kaiser test (1 min, positive); 5) coupling 1 × 30 min (activation for 2 min; Activation solution: 5 eq of PNA monomer, 4.9 eq of HBTU, 10 eq of DIPEA in dry DMF); 6) DMF wash; 7) Kaiser test (1min, negative); 8) capping 2 × 1 min; 9) DMF wash; 10) piperidine wash 2 × 2 min; 11) DMF wash; 12) DCM wash. Treatment of the dried resins with the cleavage solution (2 × 1 h) resulted in the release of the deprotected PNA oligomer. The crude sample was precipitated with 10 volumes of Et_2O at −20°C and then purified by reversed-phase HPLC (see below). The resulting aliquots of NH_2-cTnI were checked by UPLC-MS analysis and quantified by UV-vis spectrometry (see SI for details). Stock solutions of 100 μM cTnI PNA-aptamer in a 8:2

water:acetonitrile mixture were made. This was further diluted to a 10 μM concentration for deposition through click chemistry .

cTnI PNA (H - CGT GCA GTA CGC CAA CCT TTC TCA TGC GCT GCC CCT CTT A-Gly-NH_2) ε (260 nm): 396280 $M^{-1}cm^{-1}$, yield: 2.1%. UPLC-MS (ESI+, H_2O), r.t.= 2.91 min, m/z found (calculated): 1340.48 (1340.18) $[M+8H]^{8+}$; 1191.30 (1191.38) $[M+9H]^{9+}$; 1072.55 (1072.35) $[M+10H]^{10+}$. Deconvoluted mass: calculated 10713.45, found 10713.20 a.m.u. [M]. (**Figure S14**).

N_3-cTnI PNA (N_3 - CH_2CO - CGT GCA GTA CGC CAA CCT TTC TCA TGC GCT GCC CCT CTT A-Gly-NH_2) was obtained by reacting succinimidyl 2-azidoacetate with the corresponding amino precursor cTnI PNA. Succinimidyl 2-azidoacetate (5.9 mg, 3 μmol) (**Figure S13**) was reacted with a purified aliquot of cTnI PNA (30 nmol) in an Eppendorf tube. The coupling was carried out overnight in DMSO (100 μL) in the presence of DIPEA (5 μL, 30 nmol), under shaking conditions at 37°C. The resulting azido-PNA was purified with reversed-phase HPLC standard protocols, checked by UPLC-MS analysis and quantified by UV-VIS spectrometry. N_3 - CH_2CO - CGT GCA GTA CGC CAA CCT TTC TCA TGC GCT GCC CCT CTT A-Gly-NH_2, ε (260 nm): 396280 $M^{-1}cm^{-1}$, yield: 50 %. UPLC-MS (ESI+, H_2O), r.t. = 2.88 min. m/z found (calculated): 1350.46 (1350.56) $[M+8H]^{8+}$; 1200.74 (1200.61) $[M+9H]^{9+}$; 1080.86 (1080.65) $[M+10H]^{10+}$; 982.52 (982.50) $[M+10H]^{11+}$; 1080.86 (1080.65) $[M+10H]^{10+}$. Deconvoluted mass: calculated 10796.50, found 10796.0 a.m.u. [M]. (**Figure S15**).

Graphene surface modification: Graphene-TIPS was formed via electrografting of 4-((triisopropylsilyl)ethynyl)benzenediazonium tetrafluoroborate (TIPS-Eth-ArN_2^+) (10 mM) in 0.1 M tetrabutylammonium hexafluorophosphate (NBu_4PF_6) in acetonitrile using cyclic voltammetry at a scan rate of 50 mV s^{-1} for five cycles between +0.20 V and -0.60 V *vs.* Ag/AgCl. The modified electrodes were rinsed with copious amounts of acetonitrile and acetone, and gently dried. Before "click" chemistry, the TIPS protecting group was removed by immersion of graphene-TIPS surface into tetrabutylammonium fluoride (TBAF, 0.1 M in THF) for 1h at room temperature. The surface was then left for 15 min in a pure THF solution for cleaning. This modification process produces graphene-ethynyl. The deprotected surface was then exposed to azido-modified methoxypolyethylene glycol (mPEG-N_3, Mn 2.000) and azide-DNA or azide-PNA aptamer mixtures in a 2:1 ratio using $CuSO_4$ (0.01 M) and L-ascorbic acid (0.01 M) as reaction catalyst. The resulting interface was then treated with an aqueous

solution of EDTA (10 mM) for 10 min to chelate any remaining Cu^{2+} residues and finally washed copiously with water and dried under ambient conditions.

Electrical sensing: Electrical measurements were conducted using a probe station source meter unit U2322A (Keysight Technologies, USA). All measurements were performed using a PMMA commercial flow cell (Micrux Technologies, Spain) with fixed flow channel geometry (16 µL), ensuring a defined flow rate of 50 µL min^{-1} to minimize mass transport limitation of the analyte to the sensor surface in all experiments. A silver chloride wire (diameter 1 mm, Sigma-Aldrich) was used to operate the gFET device in liquid gate configuration,

Characterization: *Scanning electron microscopy (SEM)* images were obtained using an electron microscope ULTRA 55 (Zeiss, France) equipped with a thermal field emission emitter and three different detectors (ESB detector with filter grid, high efficiency In-lens SE detector and Everhart-Thornley Secondary Electron Detector). *Raman spectroscopy* measurements were performed on a LabRam HR Micro-Raman system (Horiba Jobin Yvon, France) combined with a 473 nm laser diode as excitation source. Visible light was focused by a 100× objective. The scattered light was collected by the same objective in backscattering configuration, dispersed by an 1800 mm focal length monochromator and detected by a CCD. *Electrochemical experiments* were performed on a potentiostat/galvanostat/impedance analyzer (PalmSens4, PalmSens, The Netherlands). *Surface plasmon resonance measurements* were conducted using a Biacore (T200) with a constant flow of 30 µL min^{-1}. The chips were formed by incubating 25 mM of L-cysteine on the surface for 30 min, washed and dried, followed by a solution of 10 mM 4-pentynoic acid in 1× PBS that was activated by EDC/NHS (10 and 15 mM) in 1 × PBS, for 20 min and this solution was further incubated for 2h in the cysteine-modified gold surface. The remaining ethynyl group of the 4-pentynoic acid enabled the "click" of the azido PNA (10 µM in H_2O), following the normal clicking protocol using Cu(I) as catalyst. Finally, the substrate was rinsed and washed with EDTA for 15 min, rinsed with H_2O and dried before placing it inside the SPR biacore machine. cTnI concentrations of 30, 60 and 120 pg mL^{-1} were prepared in a high and low PBS concentration with added 0.02 % Tween 20 and 1 mM $MgCl_2$.

The solutions were flushed through the gold sensor for about 15-20 min, with washing steps in between.

References

[1] T.-H. Ku, T. Zhang, H. Luo, T.M. Yen, P.-W. Chen, Y. Han, Y.-H. Lo, Nucleic Acid Aptamers: An Emerging Tool for Biotechnology and Biomedical Sensing, Sensors 15 (2015) 16281–16313.

[2] N. Nakatsuka, K.-A. Yang, J.M. Abendroth, K.M. Cheung, X. Xu, H. Yan, C. Zhao, B. Zhu, Y.S. Rim, Y. Yang, P.S. Weiss, M.N. Stonjanovic, A.M. Andrews, Aptamer–field-effect transistors overcome Debye length limitations for small-molecule sensing, Science 362 (2018) 319-324.

[3] C. Zhao, K.M. Cheung, I.-W. Huang, H. Yang, N. Nakatsuka, W. Liu, Y. Cao, T. Man, P.S. Weiss, H.G. Monbouquette, A.M. Andrews, Implantable aptamer–field-effect transistor neuroprobes for in vivo neurotransmitter monitoring, Sci. Adv. 7 (2021) eabj7422

[4] J. Daniel, S. Wedekar, K. DeCubellis, G.W. Jackson, A.S. Chiu, Q. Pagneux, H. Saada, I. Engelmann, J.L.-W. Ogiez, D., R. Boukherroub, S. Szunerits, A mask-based diagnostic platform for point-of-care screening of Covid-19, Biosens. Bioelectron. 192 (2021) 113486.

[5] M. Bianco, A. Sonato, A. De Girolamo, M. Pascale, F. Romanato, R. Rinaldi, V. Arima, An aptamer-based SPR-polarization platform for high sensitive OTA detection, Sens. Actuators B 241 (2017) 314-320.

[6] A. Abi, Z. Mohammadpour, X. Zuo, A. Safavi, Nucleic Acid-Based Electrochemical Nanobiosensors., Biosens. Bioelectron. 102 (2018) 479–489.

[7] J. Kwon, Y. Lee, T. Lee, J.-H. Ahn, Aptamer-Based Field-Effect Transistor for Detection of Avian Influenza Virus in Chicken Serum, Anal. Chem. 92 (2020) 5524–5531.

[8] L. Li, S. Xu, H. Yan, X. Li, H.S. Yazd, X. Li, T. Huang, C. Cui, J. Jiang, W. Tan, Nucleic Acid Aptamers for Molecular Diagnostics and Therapeutics: Advances and Perspectives., Angew. Chem. Int. Ed. 60 (2021) 2221–2231.

[9] F. Darfeuille, J.B. Hansen, H. Orum, C. Di Primo, J.-J. Toulmé, LNA/DNA chimeric oligomers mimic RNA aptamers targeted to the TAR RNA element of HIV-1., Nucleic Acids Res. 32 (2004) 3101–3107.

[10] A. Pasternak, F.J. Hernandez, L.M. Rasmussen, B. Vester, J. Wengel, Improved thrombin binding aptamer by incorporation of a single unlocked nucleic acid monomer, Nucleic Acids Res. 39 (2011) 1155–1164.

[11] D. Oberthur, J. Achenbach, A. Gabdulkhakov, K. Buchner, C. Maasch, S. Falke, D. Rehders, S. Klussmann, C. Betzel, Crystal structure of a mirror-image L-RNA aptamer (Spiegelmer) in complex with the natural L-protein target CCL2 Nat. Commun. 6 (2015) 6923.

[12] K.-I. Matsunaga, M. Kimoto, I. Hirao, High-Affinity DNA Aptamer Generation Targeting von Willebrand Factor A1-Domain by Genetic Alphabet Expansion for Systematic Evolution of Ligands by Exponential Enrichment Using Two Types of Libraries Composed of Five Different Bases, J. Am. Chem. Soc. 139 (2017) 324−334.

[13] K. Sefah, Z. Yang, K.M. Bradley, S. Hoshik, E. Jiménez, L. Zhang, G. Zhu, S. Shanker, F. Yu, D. Turek, W. Tan, S.A. Benner, In vitro selection with artificial expanded genetic information systems, Proc. Natl. Acad. Sci. USA 1111 (2014) 1449–1454.

[14] D. Kong, W. Yeung, R. Hili, In Vitro Selection of Diversely Functionalized Aptamers, J. Am. Chem. Soc. 139 (2017) 13977−13980.

[15] S. Arangundy-Franklin, A.I. Taylor, B.T. Porebski, V. Genna, S. Peak-Chew, A. Vaisman, R. Woodgate, M. Orozco, P. Holliger, A synthetic genetic polymer with an uncharged backbone chemistry based on alkyl phosphonate nucleic acids, Nat. Chem. 11 (2019) 533 - 5421.
[16] P. Wittung, P.E. Nielsen, O. Buchardt, M. Egholm, B. Norde'n, DNA-like double helix formed by peptide nucleic acid, Nature 368 (1994) 561–563.
[17] A. Saadati, S. Hassanpour, M. de la Guardia, J. Mosafer, M. Hashemzai, A. Mokhtarzadeh, B. Baradaran, Recent advances on application of peptide nucleic acids as a bioreceptor in biosensors development, Trends Anal. Chem. 114 (2019) 56-68.
[18] B. Cai, S. Wang, L. Huang, Y. Ning, Z. Zhang, G.-J. Zhang, Ultrasensitive Label-Free Detection of PNA–DNA Hybridization by Reduced Graphene Oxide Field-Effect Transistor Biosensor, ACS Nan 8 (2014) 2632–2638.
[19] M. Tian, M. Qiao, C. Shen, F. Meng, L.A. Frank, V.V. Krasitskaya, T. Wang, X. Zhang, R. Song, Y. Li, J. Liu, S. Xu, J. Wang, Highly-sensitive graphene field effect transistor biosensor using PNA and DNA probes for RNA detection, App. Surf. Sci. 527 (2020) 146839.
[20] T. Uno, T. Tabata, T. Kawai, Peptide−Nucleic Acid-Modified Ion-Sensitive Field-Effect Transistor-Based Biosensor for Direct Detection of DNA Hybridization, Anal. Chem. 79 (2007) 52–59.
[21] R. D'Agata, M.C. Giuffrida, G. Spoto, Peptide Nucleic Acid-Based Biosensors for Cancer Diagnosis, Molecules 22 (2017) 1951.
[22] R. D'Agata, N. Bellassai, M. Allegretti, A. Rozzi, S. Korom, A. Manicardi, E. Melucci, E. Pescarmona, R. Corradini, P. Giacomini, G. Spoto, Direct plasmonic detection of circulating RAS mutated DNA in colorectal cancer patients, Biosens. Bioelectron. 171 (2020) 112648.
[23] K.Y. Chan, A.B. Kinghorn, M. Hollenstein, J.A. Tanner, Chemical Modifications for a Next Generation of Nucleic Acid Aptamers, ChemBioChem 23 (2022) e202200006.
[24] R. Oliveira, E. Pinho, A.L. Sousa, J.J. DeStefano, N.F. Azevedo, C. Almeida, Improving aptamer performance with nucleic acid mimics: de novo and post-SELEX approaches, Trends in Biotechnol. 40 (2022) 549-563.
[25] V.V. Demidov, V.N. Potaman, M.D. Frank-Kamenetskil, E. M., O. Buchard, S.H. Sonnichsen, P.E. Nlelsen, Stability of peptide nucleic acids in human serum and cellular extracts, Biochem. Pharmacol. 48 (1994) 1310–1313.
[26] M. Schade, A. Knoll, A. Vogel, O. Seitz, J. Liebscher, D. Huster, A. Herrmann, A. Arbuzova, Remote Control of Lipophilic Nucleic Acids Domain Partitioning by DNA Hybridization and Enzymatic Cleavage, J. Am. Chem. Soc. 134 (2012) 20490−20497.
[27] V. Mishyn, A. Hugo, T. Rodrigues, P. Aspermair, H. Happy, L. Marques, C. Hurot, R. Othmen, V. Bouchiat, R. Boukherroub, W. Knoll, S. Szunerits, The holy grail of pyrene-based surface ligands on the sensitivity of graphene-based field effect transistors, Sens. Diagn. 1 (2022) 235-244
[28] Q. He, S. Wu, Z. Yin, H. Zhang, Graphene-based electronic sensors, Chem. Sci. 3 (2012) 1764–1772.
[29] C. Kotlowski, M. Larisika, P.M. Guerin, C. Kleber, T. Kröber, R. Mastrogiacomo, C. Nowak, P. Pelosi, S. Schutz, A. Schaighofer, W. Knoll, Fine discrimination of volatile compounds by graphene-immobilized odorant-binding proteins, Sens. Actuat. B 256 (2018) 564–572.
[30] T. Rodrigues, V. Mishyn, Y.R. Leroux, L. Butuille, E. Woitrain, A. Barras, P. Aspermair, H. Happy, C. Kleber, R. Boukherroub, D. Montaigne, W. Knoll, S. Szunerits, Highly performing graphene-based field effect transistor for the differentiation between mild-moderate-severe myocardial injury, NanoToday 43 (2022) 101391.

[31] A. Béraud, M. Sauvage, C.M. Bazán, M. Tie, A. Bencherif, D. Bouilly, Graphene field-effect transistors as bioanalytical sensors: design, operation and performance, Analyst 146 (2021) 403-428.
[32] S. Shaibani, L. Capua, S. Kamaei, S.S.A. Akbari, J. Zhang, H. Guerin, A.M. Ionescu, Extended gate field-effect-transistor for sensing cortisol stress hormon, Commun. Mater. 2 (2021) 10.
[33] S.S. Hah, PNA aptamer able to isolate a metal., WO2012108675A2 (2017).
[34] H.K. Lee, H.K. Lim, Y.S. Cho, S.S. Hah, Peptide Nucleic Acids Are an Additional Class of Aptamers, RSC Adv. 3 (2013) 5828-5831.
[35] X. Wang, Y. Hu, F. Qu, R.U. Khan, Multiple Modes of Capillary Electrophoresis Applied in Peptide Nucleic Acid Related Study, J. Chromatogr. A 1501 (2017) 161–166.
[36] X.Q. Wang, M. Ghulam, C. Zhu, F. Qu, Electrophoresis Reaction for Interaction Study of Amino Acid Modified Peptide Nucleic Acid and Proteins, hinese J. Anal. Chem. 46 (2018) 1895–1903.
[37] V. Galli, K.K. Sadhu, D. Masi, J. Saarbach, A. Roux, N. Winssinger, Caprin-1 Promotes Cellular Uptake of Nucleic Acids with Backbone and Sequence Discrimination Helv. Chim. Acta, 103 (2020) e19002.
[38] K. Vogel, M. Glettenberg, H. Schroeder, C.M. Niemeyer, DNA-Modification of Eukaryotic Cells, Small 9 (2013) 255-262.
[39] H. Jo, H. Gu, W. Jeon, H. Youn, J. Her, S.-K. Kim, J. Lee, J.H. Shin, C. Ban, Electrochemical Aptasensor of Cardiac Troponin I for the Early Diagnosis of Acute Myocardial Infarction, Anal. Chem. 87 (2015) 9869.
[40] V. Mishyn, T. Rodrigues, Y.R. Leroux, L. Butruille, E. Woitrain, D. Montaigne, P. Aspermair, H. Happy, W. Knoll, R. Boukherroub, S. Szunerits Electrochemical and electronic detection of biomarkers in serum: a systematic comparison using aptamer-functionalized surfaces, Anal. Bioanal. Chem. 414 (2022) 5319–5327.
[41] V. Mishyn, T. Rodrigues, Y.R. Leroux, P. Aspermair, H. Happy, J. Bintinger , C. Kleber, R. Boukherroub, W. Knoll, S. Szunerits, Controlled covalent functionalization of a graphene-channel of a field effect transistor as an ideal platform for (bio)sensing applications, Nanoscale Horiz. 6 (2021) 819-829
[42] A.C. Ferrari, D.M. Basko, Raman spectroscopy as a versatile tool for studying the properties of graphene, Nat. Nanotechnol. 8 (2013) 235–246.
[43] A. Svetlova, D. Kireev, G. Beltramo, D. Mayer, A. Offenhäusser, Origins of Leakage Currents on Electrolyte-Gated Graphene Field-Effect Transistors, ACS Appl. Electron. Mater. 12 (2021) 5355–5364.
[44] Y.R. Leroux, P. Hapiot, Nanostructured Monolayers on Carbon Substrates Prepared by Electrografting of Protected Aryldiazonium Salts, Chem. Mater. 25 (2013) 489-495.